Available online at www.sciencedirect.com
ScienceDirect
Journal of the European Ceramic Society 26 (2006) 3075–3081
www.elsevier.com/locate/jeurceramsoc

Evaluation of fracture toughness of as plasma sprayed alumina–13 wt.% titania coatings by micro-indentation techniques

R. Venkataraman *, R. Krishnamurthy

Indian Institute of Technology-Madras, Chennai 600 036, India

Received 4 February 2005; received in revised form 31 August 2005; accepted 11 September 2005
Available online 2 November 2005

Abstract

The fracture toughness of the as plasma sprayed alumina–13 wt.% titania (AT-13) coatings was evaluated using micro-indentation techniques. Indentations with smaller loads of 0.49 N show features such as partially melted particles to be extremely hard and brittle. However, the matrix made up of bi-modulus microstructure of splats was much tougher due to operative toughening mechanism for instance, crack bridging, which effectively retarded propagation of the cracks. Log plots of crack length (C) versus load (P) for loads varying from 1.96 to 9.8 N occurred with a slope of 0.65 ± 0.095 signifying sub-surface median or palmqvist type cracks to be rampant. The as sprayed microstructure made of pores; partially melted particles and splats were found to be anisotropic with regard to indentation toughness. Cracks were found to initiate and propagate easily in direction parallel to the coating growth directions than along the splat boundaries. Accordingly the bonding between the splats caused by plasma spray process could be deemed to be superior. The preferential directionality developed in the microstructure due to the imposed heat flow conditions essentially has weakened the microstructure.

Keywords: Hardness; Al_2O_3/TiO_2; Toughness; Indentation; Coatings

1. Introduction

In our earlier paper[1,15] we have reported some amount of residual α phase about 10–15% in as sprayed coatings of pure alumina which were found to be caused by unmelted or partially melted particles resulting from the initially start α phased powders. Damani et al.[2,3] have reported a very large about 35% of residual α phase in as sprayed pure alumina and in their case the starting powder size was evidently larger about 92 μm as compared to the conventional plasma spraying process powder size of less than 60 μm. Presence of partially melted powder to an extent of 10% even under careful and optimized spraying conditions is not uncommon in plasma spraying.[4–6] The partially melted particles in most cases occur due to unmelted core although other mechanisms for example splashing, rebounding from the substrate can also be equally responsible during some conditions of plasma spraying particularly for a colder substrate. Turbulence caused by voltage fluctuations or worn out anode and/or improper powder feed flow and parameters beyond the control of normal spray operations are also known to induce considerable amount of partially melted particles in the coatings.[7]

The plasma spraying of alumina–13 wt.% titania (AT-13) type coatings, in contrast with pure alumina shows a very large amount of 45–55% of residual α phase in as sprayed conditions. The residual α phase in AT-13 too can be ascribed to partially melted particles only to an extent of 10–15% as observed commonly in other type of coatings. The larger and preferential stabilization of α phase in AT-13 coatings in as sprayed coatings has been the focus of study of our earlier papers and has been attributed to the consequence of interaction of the powder in the plasma flame resulting in phase separation of titanium cations from the started powder. From our studies on plasma sprayed AT-13, it could be established that the phase separated titanium, due to difficulties in subsequent solute trapping, heterogeneously nucleates α phase in concurrence with the metastable γ phase.[8–10] The preferentially stabilized α phase thus formed by rapid solidification was found to be totally in very fine splat morphology in mesoscale dimensions of about 2–3 μm and also to be totally depleted of titanium.[11] Whereas, the partially melted particles in the coatings were generally of spherical

* Corresponding author. Present Address: National Metallurgical Laboratory, Jamshedpur 831 007, India.

0955-2219/$ – see front matter © 2005 Elsevier Ltd. All rights reserved.
doi:10.1016/j.jeurceramsoc.2005.09.054

morphology with a mixture of metastable γ and α phase and found to be abounded with titanium. In the literatures a modified version of metastable γ phase known as X-type phase, which has high solubility for titanium, was found to form as splats during rapid solidification of AT-13.[12,13] But for all of the process conditions used in this study formation of metastable X phase, as splats, could not be established.[16] Nevertheless, the preferentially stabilized α phase along with the metastable γ phase itself as splats was found to be sufficiently tough and crack resistant. However, the partially melted nearly spherical particles present to the extent of 10–15% in the as sprayed microstructure were found to be extremely hard and brittle. These divergences in fracture toughness behavior of AT-13 composite microstructure could be established from the micro-indentation study, which is the subject of this paper. In contrast with the results of this paper, in the literature, for as plasma sprayed AT-13 during bending tests, preferential crack propagation along splat boundaries and crack arresting at the partially melted spherical particles were conspicuous.[12–14] For these purposes, the results from this study may provide a clear understanding on the operative toughening mechanism for the commercially important AT-13 type composites.

Micro-indentation offers an easy and convenient method to understand the hardness and fracture toughness of brittle ceramic materials. Indentations beyond a critical load particularly on purely brittle materials tend to develop radial cracks due to the residual tensile stress arising during the unloading cycle of the indentation. The crack lengths thus created are used with semi-empirical relationship to establish the fracture toughness of the indented material.[17] While this method of estimation of fracture toughness has been in vogue for several years, it is unreliable and testing method is inconsistent and results are only about 60–75% dependable.[18,19] Yet, in this paper an attempt has been made to estimate the fracture toughness of each and every feature, by restricting the load and localizing the indentation to specific features of the microstructure, of the as sprayed AT-13 coatings using micro-indentation techniques. From, a systematic study of crack length versus load with load varying from 0.49 to 9.8 N the type of crack developing at the tip of the indentation could be established. The cracks were found to be essentially of sub-surface median or palmqvist type and not truly radial. The indentation toughness measurement also clearly indicated the anisotropy present in the fracture toughness of the microstructure. Cracks on indentation preferentially developed along the heat flow direction than parallel to the splat boundaries indicating good anchorage of splats with each other.

2. Experimental details

In all cases of plasma spraying low alloy steel substrates were used. Before usage the samples were thoroughly cleaned with acetone and shot blasted using alumina pellets. The samples after shot blasting were used immediately for spraying.

Plasma spraying was carried out with Metco-7-MG plasma spray equipment with argon as primary and hydrogen as secondary gases. In general higher operational arc voltage of 60 V with 600 A as the operating current was used during spraying. As the focus of this paper has been to understand the influence of individual features of as sprayed microstructure on the mechanical properties the processing variables have not been listed in detail. The variable coating thickness due to the nature of mechanical testing such as micro-hardness was found to be important for this paper of study and is shown as Table 1. Wherever specified, Miller-thermal (NiCrYAl) alloy powder catalog number (AI-1048) was used as bond coat material with the same operating voltage of 60 V but with lower currents of about 500 A. In all cases before spraying was attempted the powder used was preheated, baked in an oven set at 150 °C overnight and the spraying in almost all cases were completed within $\frac{1}{2}$ to 1-h after removal of the powder from the oven. In all cases starting powder was α phased only and were characterized by X-ray diffraction, SEM and BET analysis. The characteristics of the alumina–titania start powder can be specified as entirely α phased with narrow particle size distribution with an average particle size of 42 μm, with a specific surface area of 3.51 m^2/g and pore specific volume of 0.0041 cm^3/g confirming to the catalog number AI-1051 of miller thermal.

Table 1
Coating thickness of the samples

Sample number	Bond coat (μm)	Coating thickness (μm)
AT13 A1	Nil	260
AT13 A2	75–100	325
AT13 B1	Nil	250–300
AT13 B2	75–100	325–375
AT13 C	75–100	300

Samples for X-ray diffraction characterization of dimensions 10 mm × 10 mm in size were obtained by sectioning along with the substrate. X-ray diffraction was carried out with Gruber 500 X-ray diffractometer. Detailed X-ray characterization was carried out on all the samples. The X-ray diffraction pattern was collected at a scan rate of 0.02 °/s using Cu Kα radiation. In all cases the 2θ scan range were kept constant between 20 and 95°. The X-ray pattern was analyzed using FullProf[a] a program, which is based on Rietveld technique.[20] All image analysis and stereological analysis were carried out from optical microscopic images using Metal Power image analyzer software. Micro-indentation was carried out using Leica QW550 Vickers indenter with loads varying from 0.49 to 9.8 N at a loading rate of 25 g/s and for duration of 15 s.

3. Results and discussions

Typical X-ray diffraction of as sprayed samples is shown as Fig. 1. The microstructure of as sprayed samples as observed in a scanning electron microscope is shown as Fig. 2. The second phase content particularly the residual α phase was estimated from X-ray analysis by direct intensity comparison method.[10] In this method the residual α phase ratio is estimated simply after background subtraction, from the maximum intensity of

[a] FullProf (Version-3.5, DEC97, -Laboratorie leon brillouin (cea-cnrs)).

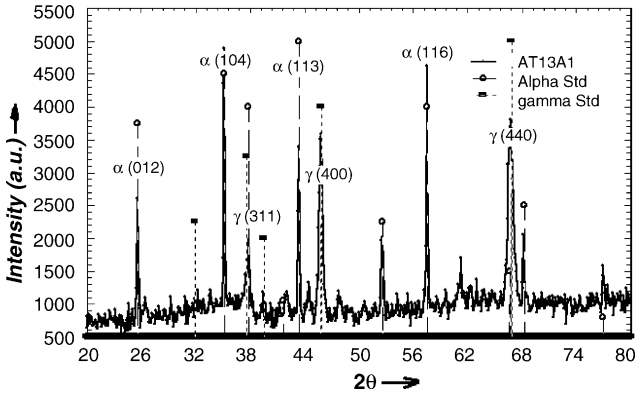

Fig. 1. Typical X-ray diffraction from as sprayed samples of alumina–13 wt.%Titania.

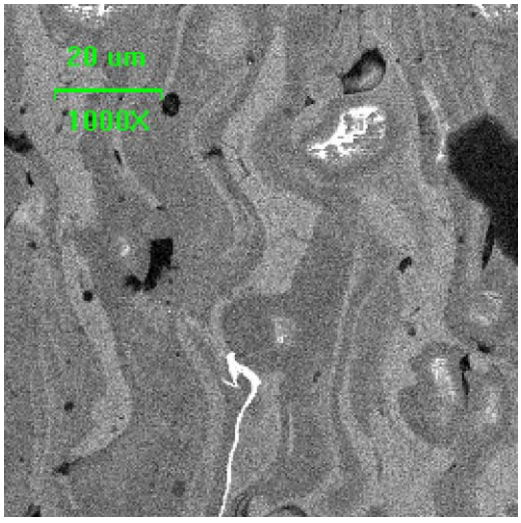

Fig. 2. A typical scanning electron microstructure of as plasma sprayed AT-13 coatings.

the intense peaks of the metastable γ and residual α phase and is shown as Eq. (1).

$$\frac{\text{X-ray intensity value from the intense peak of } \alpha \text{ phase}}{\text{X-ray intensity value from the intense peak of } (\alpha \text{ phase} + \gamma \text{ phase})} \quad (1)$$

As seen from Fig. 1 and comparing with the microstructure of Fig. 2, it can be inferred that the intensity of residual α phase estimated by X-ray analysis does not distinguish between the α phase occurring in splat morphology or partially melted α phase occurring as nearly spherical particles.

These particles on some occasions were also found to be a mixture of metastable γ and α phase due to partial rapid solidification.[12] Hence, from X-ray intensities alone it is not possible to distinguish the quantity of each and every feature of the microstructure. Phase estimation was hence attempted with image and stereological analysis using an optical microscope. Table 2 shows the estimation of the residual α phase from X-ray and image analysis. As seen in Table 2, as expected, there is a wide difference in the values of residual α phase from these two methods of estimation. By using the area fraction analysis of image analyzer software and by restricting the threshold limits, residual α phase occurring in splat morphology alone could be estimated. The values shown in Table 2 were obtained from an average of 16 fields of size 0.222 mm^2 each. The average values reported in each of the samples are within 10–15% of the maximum and minimum values of the 16 frames. Hence, the value from image analysis is a good representation of the residual α second phase occurring as splats. But by image analysis too the volume fractions of important features such as partially melted particles could not be estimated. Consequently, for these microstructures volume fraction estimation for partially melted particle was determined by applying stereological relationship $V_v = L_l$, where L_l denotes the total intersection length of a specific feature with a test line L_t per unit length of the latter.[21] However, it is to be noted that, as observed in the transmission electron microscopy studies these partially melted particles are also indeed a mixture of metastable γ and α phase only.[13] But for this study these particles in a broader sense was assumed to be totally of residual α phase only. A detailed transmission electron microscopy study is underway without which it is not possible to identify the extent of each of the phases present in these particles. From stereological analysis the spatial distribution of the phase domains of the partially melted particles was also determined by estimating the mean free path and mean particle size of the features and is shown in Table 3.[22] As observed in the Table 3 the mean particle size of the partially melted particles were less than 12 μm, which in comparison to the starting particle size of 45 μm signifies unmelted core only. Notwithstanding the process variables as seen in Table 3, a general trend that is conspicuous is that the partially melted particles are evenly distributed with very less contiguity and with a mean free path of at least 100 μm, i.e. about 10 times the mean size of the particles. In Table 3 the values as seen in five frames has been reported as

Table 2
Second phase and partially melted particle estimation by image analysis and X-ray techniques

Sample number	Max intensity of α phase	Max intensity of γ phase	Residual α phase ratio from Eq. (1)	Residual α phase as splat from image analysis	Residual α phase as PMP's from linear intercept
AT13A1	α (104)–1900	γ (400)–1470	0.56	0.28	0.103
AT13A2	α (104)–1247	γ (400)–956	0.57	0.25	0.111
AT13B1	α (113)–2187	γ (440)–1775	0.56	0.27	0.092
AT13B2	α (104)–1242	γ (400)–875	0.59	0.25	0.121
AT13 C	α (113)–1960	γ (400)–1048	0.65	–	–

Table 3
Particle size and mean free path analysis using stereological techniques

Sample ID	Parameter	Frame 1	Frame 2	Frame 3	Frame 4	Frame 5
AT13 A1	V_v	0.089	0.1004	0.1372	0.0808	0.107
	$\bar{d}$(μm)	14.5	9.1	7.9	12.31	9.12
	N_L (mm^{-1})	6.90	10.96	12.59	8.12	10.96
	λ (μm)	130	82	68.5	113.2	81.4
AT13 A2	V_v	0.111	0.111	0.098	0.115	0.122
	$\bar{d}$(μm)	9.12	8.49	11.19	8.49	8.49
	N_L (mm^{-1})	10.96	11.78	8.93	11.78	11.78
	λ (μm)	81.1	75.4	101.1	75.1	74.5
AT13 B1	V_v	0.118	0.103	0.079	0.16	–
	$\bar{d}$(μm)	8.80	12.96	14.49	6.84	–
	N_L (mm^{-1})	11.37	7.72	6.903	14.62	–
	λ (μm)	77.6	116.2	133.5	57.5	–
AT13 B2	V_v	0.155	0.117	0.098	0.115	0.118
	$\bar{d}$(μm)	6.84	8.80	11.19	9.12	10.26
	N_L (mm^{-1})	14.62	11.37	8.93	10.96	9.75
	λ (μm)	57.8	77.6	101.1	80.7	90.5

such and not the average value so as to have a feel in the spread of the observed values.

3.1. Micro-indentation studies

The microstructural features such as pores, partially melted particles, splats of the as sprayed coatings were consistent in all the coatings irrespective of the processing conditions although the quantity of individual features differed from one specimen to other. Micro-indentation studies typically were carried out in two sets of experiments. In the first of these, the loads were varied only between 0.49 and 1.96 N and fracture toughness of individual features present in the microstructure were estimated and are shown as Table 4. Whereas, in the second set loads were varied between 1.96 and 9.8 N and the nature of cracking at the indentation tip of the overall structure was estimated and is shown as Table 5. From the latter set of experiments the anisotropy in fracture toughness prevalent in the matrix and the type of crack developing at the indent could be clearly delineated. As seen in Table 4, typically irrespective of the experimental conditions, indentation on features such as partially melted particles with loads ranging from 0.49 to 1.96 N has resulted in an average indentation hardness value of 1850 HV. The hardness values of the α phased splats appearing white in contrast and the metastable γ phased matrix was similar and an average value of 1500 HV could be measured.

For load range of 0.49–1.96 N the cracking observed in the microstructure were typically of three types:

(a) When indentation loads were restricted to low values of 0.49 N and the area of focus was on partially melted particles only as shown in Fig. 3(a), the indentation was improper due to the downward moment of loosely fit partially melted particles. During relaxation of the indentation the partially melted particles was found either to crack or detach from the matrix due to the poor mechanical anchorage to the matrix.
(b) When indentation was focused on the matrix and loads were reasonably high about 0.98 N as shown in Fig. 3(b), the

Table 4
Indentation and fracture toughness values of specific features of typical microstructure shown as Fig. 2

Features	Load in grams	Indentation length in (μm)	Hardness (HV)	Hardness (GPa)	Crack length (a) (μm)	Fracture toughness (MPa $\sqrt{m}$)
Matrix	100	11.25	1500	14.36	16.6	1.06
Matrix	100	11.25	1500	14.36	13.8	1.40
Matrix	50	8.5	1300	12.58	9.5	1.31
PMP's	100	9.5	2000	20.14	22.12	0.58
PMP's	50	7.4	1870	16.59	15.25	0.56

Table 5
Crack length, fracture toughness vs. load for directions perpendicular (⊥) and parallel (Ξ) to the splat boundaries

Load (gf)	Hardness (GPa)	Crack length ⊥ (μm)	Crack length Ξ (μm)	Fracture toughness (⊥) (MPa $\sqrt{m}$)	Fracture toughness (Ξ) (MPa $\sqrt{m}$)
200	11.41	17	–	2.30	–
300	11.06	18	11	3.21	6.21
500	10.73	29	20	2.66	4.64
1000	8.26	45	42	3.15	3.47

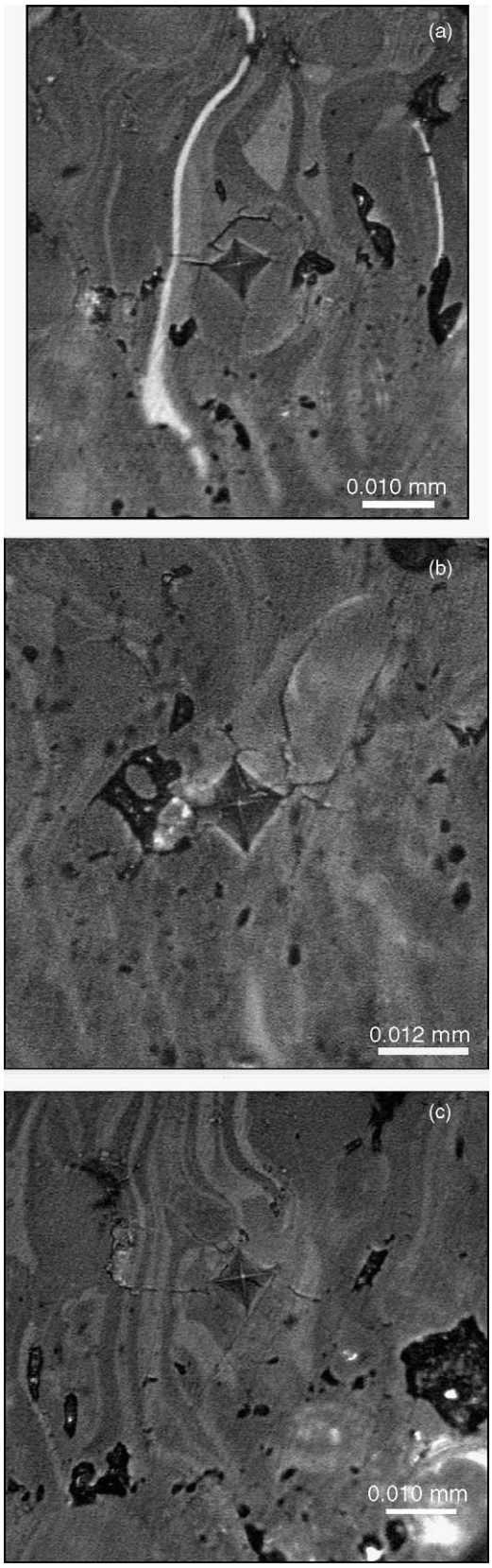

Fig. 3. (a–c) Typical micro-indentation on as sprayed samples. The indentation can be classified as three types: (a) preferential cracking of PMP's when indentation restricted on PMP's (b) cracking of brittle PMP's when indentation focused on areas of matrix but close to partially melted particles (c) crack bridging and illustration of tougher matrix when indentation was purely on matrix.

indentation was perfect as seen by the symmetrical diagonals of the indentation. The cracks emanating from the tip of the indentations were branched due to the toughness of the matrix and in particular due to the tougher α phase observed as white in contrast. Partially melted particles even though located far away from the indentation spots were found to crack or break away from the matrix due to its brittleness.

(c) When indentation was carried out at moderate loads of about 1.96 N on the matrix toughening mechanism for example crack bridging were found to be operative. This is shown as Fig. 3(c).

A rough estimate of fracture toughness can be made from the cracks emanating at the tip of the indentation using an empirical relationship.[17]

$$K_C = \chi\left(\frac{E}{H}\right)^{1/2}\frac{P}{a^{3/2}} \quad (2)$$

where $\chi = 0.016$, an empirical constant based on the indenter type and geometry; E is the elastic modulus about 300 GPa for the ceramic material of study[23]; H is the hardness in GPa; P is the load applied in N; and 'a' is the crack length in meters measured from the center of the indent. Table 4 shows the values of fracture toughness observed for the various features of the mesostructure.

This method of estimation of fracture toughness using indentation techniques can be severally limited due to various factors. First of all the geometrical constant used in the semi-empirical equation is approximate only and it depends on the indentation geometry and its reliability of even properly indented specimens is only about 60–75%.[17] In our calculation a value of 0.016 the most accepted value for this constant has been used for calculation. In many cases values as high as 0.031 has been cited.[24] In our case some of the indentation particularly on partially melted particles was not of perfect square shape, because even at low loads the partially melted particle was found to give away as these were loosely held to the matrix. Further, the bi-modulus microstructure, as observed in Fig. 3(c) was easily toughened by crack bridging mechanisms. The indentation technique is not applicable for bridging type ceramics, as the estimation of crack length is erroneous.[17] Although, the microstructure is made of metastable γ and residual α phase, which is at least two to three times stiffer than the former, a single value of elastic modulus has been roughly used in the estimation of fracture toughness.[3] Accordingly, the values of fracture toughness reported here is slightly an over estimate especially for the matrix. Further Eq. (2) is suitable for situations where the material is totally brittle and radial cracks limited to surface only should develop during the unloading cycle of the indentation. To have a right estimate of fracture toughness by indentation method load values have to be chosen so that the c/a ratio, where 'c' is the crack length and 'a' the length of half indentation diagonal should be at least 2.5 times.[19] But testing at these conditions would have to be at very high loads and in such a situation the purpose of micro-indentation study will be lost. Hence, the estimation

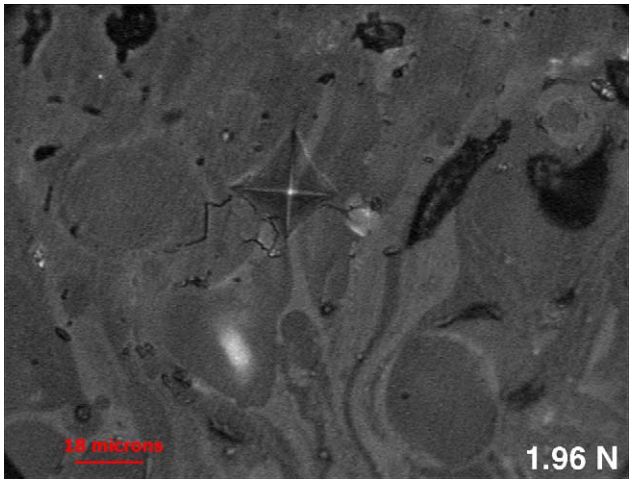

Fig. 4. Typical micro-indentation at a load of 1.96 N. The cracks tend to initiate very easily and preferentially propagate along directions perpendicular to splat boundaries.

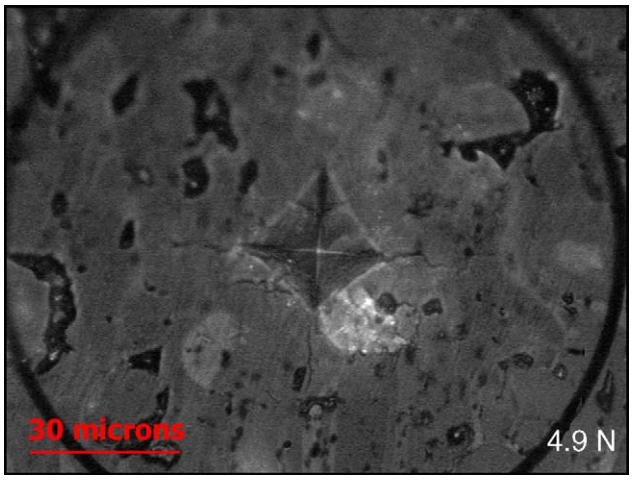

Fig. 5. Typical micro-indentation at a load of 4.9 N. The cracks tends be anisotropic with larger crack length along direction perpendicular than along splat boundaries.

of fracture toughness by micro-indentation techniques gives an approximate value only, but definitely could be used for comparison purposes between two constituent features within the microstructure over similar load range.

In situations of quasi-brittle materials to understand the nature of the cracks developing during indentation a systematic study of crack length (C) versus load (P) is necessary. Hence, micro-indentation studies were carried out with loads varying from 1.96 to 9.8 N. Table 5 shows the values of fracture toughness that could be estimated from these tests.

The common features for the load range of 1.96–9.8 N are:

(a) As seen in this Table 5 the hardness and fracture toughness values for all loads corresponds to the overall structure only.
(b) The cracking appears to be preferential. Cracks tend to emanate easily at lower loads of 1.96 N itself along direction parallel to the coating build up which is shown as Fig. 4 and Table 5. Further the crack length observed is also larger along the coating build up directions as compared to the directions parallel to the splat boundaries for all loads and a typical example is shown as Fig. 5 for a moderate load of 4.9 N.
(c) Fig. 6 shows the log (C) versus log (P) plot. A linear fit of this plot gives a slope of 0.65 ± 0.095 with an R-value of 0.98. This value closely corresponds to the value of 0.67 commonly cited in the literature for the sub-surface type a median (half-penny) or palmqvist crack system.[25] Unlike radial cracks, the fact that the sub-surface cracks develop during the loading cycle of the indentation results in a marked difference in the plots of crack length versus load.[26]
(d) As seen in Table 5 hardness seems to be dependent on the load applied. In consideration of this fact it is necessary to establish the crack free true hardness value. In a logical sense it is not possible to establish the true hardness as well as the fracture toughness from the same Vickers micro-indentation. Li et al.[25] have used crack free, relaxation corrected, knoop indentation hardness measurements to calculate the true hardness of the material.

Central to the micro-indentation analysis of this paper is the complicated nature of the as sprayed microstructure of the coatings. The fact that the microstructure is made of at least four features such as porosity, partially melted particles, bi-modulus splats offers a genuine motive for micro-indentation studies. The fracture toughness values if when analyzed in conjunction with the stereological analysis of the as sprayed coatings advocates that the presence of hard and brittle partially melted particles allows easy initiation of cracks. The ensuing crack propagation is fully retarded due to the fact that the brittle particles are present with a wide dispersion with little contiguity and with a mean free path between particles at least 10 times more than the average particle size. In a separate study focused on adhesive strength measurement by cross-hatch testing method the matrix although anisotropic was found to be sufficiently tough to with-

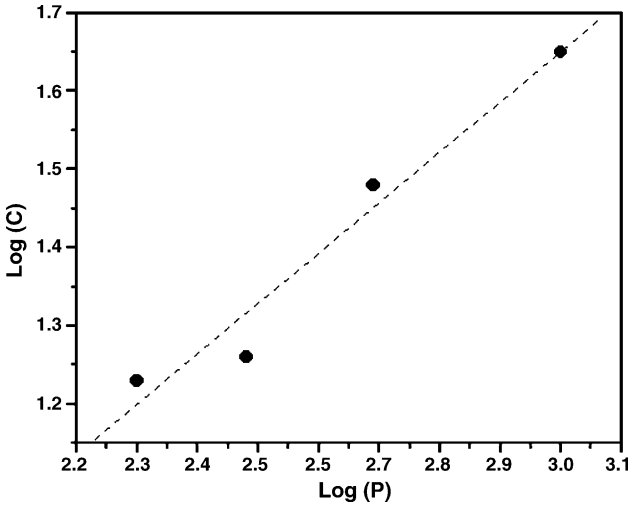

Fig. 6. Plot of log (C) vs. log (P) for a load range from 1.96 to 9.8 N. The linear fit for this plot occurs with a slope of 0.65 ± 0.095 with an R-value of 0.98.

stand crack initiation and could show high adhesive strength despite the presence of partially melted particles. In contrast with this situation, pure alumina coatings in a similar type of testing method showed very poor adhesive strength. Microcracking in the matrix and easy crack propagation seemed to be the major cause of poor adhesive strength of pure alumina coatings.[1,15]

4. Conclusions

(a) Plasma sprayed AT-13 coatings in as sprayed coatings were of complicated microstructure formed with at least four salient features. Partially melted particles occurring to the extent of 10–15% in volume was very well dispersed in the microstructure with little contiguity and with a mean free path of at least 10 times its mean particle size irrespective of the processing conditions used in this study.
(b) The matrix made of bi-modulus microstructure in the splat morphology was found to be extremely anisotropic with regard to fracture toughness. Cracks were found to initiate at lower loads and propagate to longer distance along directions perpendicular to splat boundaries.
(c) The partially melted particles were found be extremely hard, brittle and loosely anchored to the matrix for all experimental conditions studied.
(d) Cracks during micro-indentation were found to form specifically of sub-surface half-penny palmqvist type and preferentially occurred during loading cycle of the indentation.

Acknowledgments

The authors wish to thank staff of Plasma spray unit and staff of Micro-Indentation Laboratory, specifically Dr. B. Venkataraman, Defense Metallurgical Laboratory, Hyderabad for all the help provided during plasma spraying and micro-indentation measurements. One of the author, R. Venkataraman wishes to acknowledge the Director, National Metallurgical Laboratory, Jamshedpur, India for permitting him to work on this paper.

References

1. Venkataraman, R., Sampath Kumar, T. S. and Krishnamurthy, R., Study on absence of influence of residual α phase on adhesive/cohesive strength of as plasma sprayed pure alumina coatings evaluated by ASTM D 3359-B cross-hatch testing method. *Surf. Coat. Technol*., submitted for publication.
2. Damani, R. J. and Wanner, A., Microstructure and elastic properties of plasma sprayed alumina. *J. Mater. Sci.*, 2000, **35**, 4307–4314.
3. Damani, R. J. and Makroczy, P., Heat treatment induced phase and microstructural development in bulk plasma sprayed alumina. *J. Eur. Ceram. Soc.*, 2000, **20**, 867–888.
4. McPherson, R., On the formation of thermally sprayed alumina coatings. *J. Mater. Sci.*, 1980, **15**, 3141–3147.
5. Trice, R. W. and Faber, K. T., Role of lamellae morphology on the microstructure and mechanical properties of plasma sprayed alumina. *J. Am. Ceram. Soc.*, 2000, **83**, 889–894.
6. Sampath, S., Gansert, R. and Herman, H., Plasma-spray forming ceramics and layered composites. *J. Metal.*, 1995, **47**, 30–36.
7. Vardelle, M. and Fauchais, P., Plasma spray process diagnostics and control? *Pure Appl. Chem.*, 1999, **71**, 1909–1918.
8. Venkataraman, R., Singh, P. and Krishnamurthy, R., Enhanced α phase stability observed in as-sprayed alumina–13 mol% titania on plasma spraying. *J. Am. Ceram. Soc.*, in press.
9. Venkataraman, R., Sampathkumar, T. S., Krishnamurthy, R., Das, D. K. and Venkataraman, B., Analysis of α phase content of as sprayed pure alumina and alumina–13 wt.% titania plasma sprayed coatings on low alloy steel substrates. *J. Surf. Coat. Technol.*, submitted for publication.
10. Venkataraman, R., *Study on the Phase Stability and Correlation to the Adhesive Strength of as Plasma Sprayed Oxide Ceramic Coatings*. Ph.D. thesis, IIT-Madras, Chennai, India, 2003.
11. Colaizzi, J., Mayo, W. E., Kear, B. H. and Liao, S. C., Dense nanoscale single and multi-phase ceramics sintered by transformation assisted consolidation. *Int. J. Powder Metall.*, 2001, **37**, 45–54.
12. Jordan, E. H., Gell, M., Sohn, Y. H., Goberman, D., Shaw, L. and Xiao, T. D., Fabrication and evaluation of plasma sprayed nanostructured alumina–titania coatings with superior properties. *Mater. Sci. Eng. A*, 2001, **301**, 80–89.
13. Goberman, D., Sohn, Y. H., Shaw, L., Jordan, E. H. and Gell, M., Microstructure development of Al_2O_3–TiO_2 plasma sprayed coatings derived from nanocrystalline powders. *Acta Mater.*, 2002, **50**, 1141–1152.
14. Gell, M., Jordan, E. H., Sohn, Y. H., Goberman, D., Shaw, L. and Xiao, T. D., Development and implementation of plasma sprayed nanostructured ceramic coatings. *Surf. Coat. Technol.*, 2001, **146/147**, 48–54.
15. Venkataraman, R., Sampathkumar, T. S., Krishnamurthy, R., Das, D. K. and Venkataraman, B., Evaluation of adhesive strength measurements of plasma spray coatings by modified cross hatch (ASTM D 3359-B) testing method. *J. Thermal Spray Technol.*, in press.
16. Venkataraman, R., Ravikumar, B. and Krishnamurthy, R., A study on phase stability observed in as sprayed alumina–13 wt.% titania coatings grown by detonation gun and plasma spraying on low alloy steel substrates. *Mater. Characterizat.*, submitted for publication.
17. Jamie, J. K. and Ritchie, R. O., Determining the toughness of ceramics from Vickers indentations using the crack-opening displacements: an experimental study. *J. Am. Ceram. Soc.*, 2003, **86**, 1433–1436.
18. Ansistis, G. R., Chantikul, P., Lawn, B. R. and Marshall, D. B., A critical evaluation of indentation techniques for measuring fracture toughness-I, direct crack measurements. *J. Am. Ceram. Soc.*, 1981, **64**, 533–538.
19. Bisrat, Y. and Roberts, S. G., Residual stress measurements by hertzian indentation. *Mater. Sci. Eng. A*, 2000, **288**, 148–153.
20. Wiles, D. B. and Young, R. A., *J. Appl. Cryst.*, 1981, **14**, 149.
21. Underwood, E. E., Quantitative metallography. In *Metals Handbook. Metallographic and Microstructures* (*Vol. 9*, *9th ed.*). American Society for Metals, Ohio, 1985, pp. 123–132.
22. Messner, C., Silberschmidt, V. V. and Werner, E. A., Thermally induced surface roughness in austenitic–ferritic duplex stainless steels. *Acta Mater.*, 2003, **51**, 1525–1537.
23. Gill, S. C. and Clyne, T. W., Investigation of residual stress generation during thermal spraying by continuous curvature measurement. *Thin Solid Films*, 1994, **250**, 172–180.
24. Volinsky, A. A., Vella, J. B. and Gerberich, W. W., Fracture toughness, adhesion and mechanical properties of low-K dielectric thin films measured by nanoindentation. *Thin Solid Films*, 2003, **429**, 201–210.
25. Li, Z., Ghosh, A., Kobayashi, A. S. and Bradt, R. C., Indentation fracture toughness of sintered silicon carbide in the Palmqvist crack regime. *J. Am. Ceram. Soc.*, 1989, **72**, 904–911.
26. Lawn, B. R., Evans, A. G. and Marshall, D. B., Elastic/Plastic indentation damage in ceramics: the median/radial crack system. *J. Am. Ceram. Soc.*, 1980, **63**, 574–581.